Structural Concrete
Journal of the *fib*

Parametric numerical study on service-load deflections of reinforced recycled aggregate concrete slabs and beams based on *fib* Model Code 2010

Journal:	*Structural Concrete*
Manuscript ID	suco.202000015.R2
Wiley - Manuscript type:	Technical Paper
Date Submitted by the Author:	n/a
Complete List of Authors:	Tošić, Nikola; Universitat Politecnica de Catalunya, Civil and Environmental Engineering Department Kurama, Yahya; University of Notre Dame, Department of Civil and Environmental Engineering and Earth Sciences
Subject codes:	fib Model Code 2010, analysis and design methods, standards, regulations, guidelines, directives, building materials | construction materials
Keywords:	recycled aggregate concrete, deflection, numerical analysis, OpenSees, fib Model Code 2010
Abstract:	Recycled aggregate concrete (RAC) is entering into structural design codes such as the new Eurocode 2. However, serviceability limit state (SLS) behaviour of RAC, especially deflections, can be significantly greater than for natural aggregate concrete (NAC). Proposals for deflection control of RAC exist, but there still have not been significant studies on their implications for SLS design. In this paper, a comprehensive numerical parametric study on the sustained service-load deflections of reinforced RAC slabs and beams is described. First, a concrete material model for the time-dependent analysis of reinforced concrete structures is described, validated, and calibrated, incorporating fib Model Code 2010 creep and shrinkage models in the OpenSees structural analysis program. Then, service-load deflection analyses are conducted on RAC one-way slabs and T-beams considering the amount of coarse recycled concrete aggregate (RCA), concrete strength class, element height, span, statical system, relative humidity, and quasi-permanent load–to–design load ratio. The results show that RCA begins to have an appreciable effect on deflections only for coarse aggregate replacement percentages above 25%. At 50% replacement, the maximum spans to satisfy deflection limits can be considerably reduced; however, these reductions are smaller for T-beams and higher class concrete. The results confirm the versatility of the numerical model, applicability, and limitations of RAC in SLS design.

Parametric numerical study on service-load deflections of reinforced recycled aggregate concrete slabs and beams based on *fib* Model Code 2010

Running Head: Parametric study on deflections of RAC elements

Nikola Tošić[a,*], Yahya Kurama[b]

[a] *Civil and Environmental Engineering Department, Universitat Politècnica de Catalunya (UPC), Jordi Girona 1–3, 08034 Barcelona, Spain*
[b] *Department of Civil and Environmental Engineering and Earth Sciences, University of Notre Dame, Notre Dame, IN, USA*

* Corresponding author. Tel.: +34 93 401 78 25
E-mail address: nikola.tosic@upc.edu
Postal address: Civil and Environmental Engineering Department, Universitat Politècnica de Catalunya (UPC), Jordi Girona 1–3, 08034 Barcelona, Spain
Yahya Kurama
E-mail address: ykurama@nd.edu

ABSTRACT

Recycled aggregate concrete (RAC) is entering into structural design codes such as the new Eurocode 2. However, serviceability limit state (SLS) behaviour of RAC, especially deflections, can be significantly greater than for natural aggregate concrete (NAC). Proposals for deflection control of RAC exist, but there still have not been significant studies on their implications for SLS design. In this paper, a comprehensive numerical parametric study on the sustained service-load deflections of reinforced RAC slabs and beams is described. First, a concrete material model for the time-dependent analysis of reinforced concrete structures is described, validated, and calibrated, incorporating *fib* Model Code 2010 creep and shrinkage models in the OpenSees structural analysis program. Then, service-load deflection analyses are conducted on RAC one-way slabs and T-beams considering the amount of coarse recycled concrete aggregate (RCA), concrete strength class, element height, span, statical system, relative humidity, and quasi-permanent load–to–design load ratio. The results show that RCA begins to have an appreciable effect on deflections only for coarse aggregate replacement percentages above 25%. At 50% replacement, the maximum spans to satisfy deflection limits can be considerably reduced; however, these reductions are smaller for T-beams and higher class concrete. The results confirm the versatility of the numerical model, applicability, and limitations of RAC in SLS design.

Keywords:

Recycled aggregate concrete; deflection; numerical analysis, OpenSees; Model Code 2010

1. Introduction

With a global annual production of over 20 billion tons (WBCSD, 2009), concrete consumes immense amounts of natural resources, such as river rock and crushed stone (Tam et al., 2018). Further, the construction of new concrete structures and demolition of existing ones lead to significant amounts of construction and demolition waste (CDW), e.g., in the EU, over 850 million tons every year (Fisher and Werge, 2011). To mitigate these effects, researchers have been investigating the use of recycled concrete aggregate (RCA), obtained by crushing and sieving concrete waste (Nixon, 1978), to make new concrete, called recycled aggregate concrete (RAC). In order to improve the sustainability of the concrete industry, RAC must find its way for widespread use, and especially in structural applications, as the environmental and economic benefits of this material have been demonstrated (Azúa et al., 2019; Tošić et al., 2015).

When concrete waste is crushed, some amount of cement mortar remains attached to the natural aggregate (NA), thus causing higher porosity, higher water absorption, and lower density of RCA. Researchers have investigated the effects of this 'residual' mortar as well as other characteristics related to the manufacturing of RCA (e.g., variability of source concrete) on the physical-mechanical and durability properties of RAC as well as the structural behaviour of reinforced RAC elements in comparison with natural aggregate concrete (NAC).

There have been especially comprehensive studies and reviews at the material level (Carević et al., 2019; Ignjatović, 2013; Li, 2009; Silva, 2015). Because of the extremely high water absorption of fine RCA (<4 mm), studies have mostly focused on RAC, in which coarse NA is replaced with coarse RCA (>4 mm). In terms of the main mechanical and durability-related properties, the effects of RCA on the compressive and tensile strengths of concrete are moderate (Pacheco et al., 2019), with slightly lower resistance to carbonation (Carević et al., 2019). However, the effects are much greater in decreased modulus of elasticity of RAC (Silva et al., 2016), and in terms of time-dependent properties such as creep and shrinkage strains, both of which increase significantly with RCA content in RAC (Knaack and Kurama, 2015a; Lye et al., 2016b, 2016a).

A large number of studies has also been performed on the structural behavior of RAC, from tests on reinforced and prestressed beams in shear and flexure (Brandes and Kurama, 2018a; Fathifazl et al., 2010; Knaack and Kurama, 2014; Tošić et al., 2016) to static lateral pushover tests (Pacheco et al., 2015) and shake-table tests (Xiao et al., 2012). Regarding the ultimate limit state (ULS) behavior of RAC elements, no significant differences were found relative to NAC. However, large differences were observed in the serviceability limit state (SLS) behavior; specifically, in terms of increased deflections of RAC beams in sustained load tests (Brandes and Kurama, 2018b; Knaack and Kurama, 2015b; Seara-Paz et al., 2018; Tošić et al., 2018b). These differences have been attributed to the decreased modulus of elasticity, increased shrinkage, and increased creep of RCA, but also to potentially reduced tension-stiffening effects (Santana Rangel et al., 2017).

This significant body of research is finally being translated into design guidelines. For example, the new revision of Eurocode 2 (PT1prEN1992-1-1, 2017) will contain provisions for the structural design of RAC. Proposals have been put forward for the adjustment of existing NAC SLS design guidelines to RAC, such as for the modulus of elasticity, creep coefficient, shrinkage strain, as well as the ζ-method for deflection control (Tošić et al., 2019a, 2019d, 2018a). Although these adjustments allow the SLS design of RAC, the formulations are based on a limited number of experimental results and need further analysis, especially in the case of long-term deflections. Therefore, the aim of the study described in this paper is to introduce a reliable numerical tool for the analysis of the time-dependent behavior of reinforced RAC elements based on the *fib* Model Code 2010 (FIB, 2013), and study the SLS design implications of using RAC in beams and slabs.

For this purpose, a concrete material model, recently developed together with a new creep analysis procedure (Knaack and Kurama, 2018) within the OpenSees structural analysis framework (McKenna, 2011), was revised to conform to the *fib* Model Code 2010 creep and shrinkage relationships. The revised model was first validated and calibrated on experimental long-term deflections of RAC and NAC elements. Then, it was used to perform a parametric study on the sustained service-load deflection behaviour of reinforced RAC slabs and beams in terms of the volumetric replacement percentage of coarse NA with RCA and considering different load levels, statical systems, element spans and sizes, as well as concrete class and relative humidity.

2. Modelling time-dependent behaviour of concrete in OpenSees

2.1. TDConcreteMC10NL material model and time-dependent analysis procedure

OpenSees is an object-oriented open-source structural analysis software (McKenna, 2011) that allows users to develop new capabilities, material models, and element types. Although mostly used for dynamic analysis and earthquake engineering, the Static Analysis procedure in OpenSees (Mazzoni et al., 2006) uses a 'pseudo-time' concept that associates time with the analysis domain. For example, if a 'pseudo-time' step of

0.1 days is prescribed to reach a force F after 1 day, then 10 steps of 0.1 days, each with a $0.1 \cdot F$ force increment will be required. This property of the Static Analysis procedure in OpenSees was taken advantage of for modelling time-dependent behaviour of concrete, by introducing a global variable "set Creep" (set to 1 or 0) that would be recognized by time-dependent concrete material models.

In their work, Knaack and Kurama (2018) used the fibre element and Concrete02 material in OpenSees (Mazzoni et al., 2006) to develop a new concrete material, TDConcrete, that includes time-dependent creep and shrinkage strains. TDConcrete has linear behaviour in compression, shrinkage and creep behaviours based on ACI 209R-92 (1992), and post-cracking behaviour based on the tension-stiffening model by Tamai et al. (1988) as:

$$\sigma_{ct} = f_{ctm} \cdot \left(\frac{\varepsilon_{ct,m}}{\varepsilon_m}\right)^{b_{ts}} \tag{1}$$

where, f_{ctm} is the mean axial tensile strength, $\varepsilon_{ct,m}$ is the tensile strain at cracking, ε_m is the current tensile strain, σ_{ct} is the concrete tensile stress, and b_{ts} is a tension-softening parameter (originally proposed as 0.4 by Tamai et al., 1988). Full information on the TDConcrete material model, with source code and example files, is available in Knaack (2013).

For the current study, a revised concrete material model, TDConcreteMC10NL, was developed based on TDConcrete as follows. First, instead of linear behaviour, TDConcreteMC10NL uses a nonlinear relationship for concrete in compression, taken from the existing Concrete02 model in OpenSees (Mazzoni et al., 2006; Mohd-Yassin and Filippou, 1994). Second, for shrinkage and creep strains, TDConcreteMC10NL uses the relationships of the *fib* Model Code 2010 (FIB, 2013), separating them into basic and drying components. Hence, TDConcreteMC10NL defines the total concrete strain (without considering thermal strains) as

$$\varepsilon_{tot}(t_s,t_0,t) = \varepsilon_m(t) + \varepsilon_{cbc}(t,t_0) + \varepsilon_{cdc}(t,t_0) + \varepsilon_{cbs}(t) + \varepsilon_{cds}(t,t_s) \tag{2}$$

where, ε_{tot} is the total strain, ε_m is the mechanical strain, ε_{cbc} and ε_{cdc} are the basic and drying creep strains, respectively, ε_{cbs} and ε_{cds} are the basic and drying shrinkage strains, respectively, t is the current time, t_s is the age of concrete at the start of drying, and t_0 is the age of concrete at loading.

Once the global variable "setCreep" is set to 1 in the Static Analysis, the material model begins accumulating shrinkage and creep strains under the following time-dependent analysis procedure: first, the shrinkage strain for each fibre of the element is determined based on the current time t and the age at the start of drying t_s; then, the creep strain is calculated using the fibre stress from the previous analysis step; the mechanical strain is calculated using Eq. (2) by subtracting the shrinkage and creep strains from the total strain obtained in the previous step; and finally, stress is calculated from the compressive and tensile constitutive equations. Once stresses are determined for all of the fibres, they are integrated within the cross-section to determine the internal forces and check convergence of the unbalanced force vector in the global analysis. Note that this procedure is the same as that described for "Creep Analysis" in Knaack and Kurama (2018) and Knaack (2013), but is now accomplished using "setCreep" as part of the Static Analysis in OpenSees.

The input parameters for the TDConcreteMC10NL material are the concrete compressive strength, ultimate (crushing) strength, strain at crushing, tensile strength, modulus of elasticity at 28 days and at age of first loading, tension-softening parameter b_{ts} from Eq. (1), age at start of drying (minimum 2 days), and creep and shrinkage constitutive parameters based on the *fib* Model Code 2010 (FIB, 2013). A User Manual for TDConcreteMC10NL, together with several example files, are available in the form of Mendeley Data (Tošić et al., 2019b). Additionally, the source code for TDConcreteMC10NL can be found at https://github.com/ntosic87/OpenSees (Tošić et al., 2019c), using this code, users can create an executable file with the necessary capabilities for modelling time-dependent concrete behaviour in OpenSees.

2.2. Validation of TDConcreteMC10NL

To validate the capabilities of the TDConcreteMC10NL material model, experimentally-measured deflection curves of two reinforced NAC beams (B1a and B1b) and two NAC slabs (S1a and S1b) from Gilbert and Nejadi (2004) were modelled. These specimens were tested with a 3.5-m span in four-point bending for 380 days under varying ratios of sustained load to ultimate load. The numerical analyses were performed using the measured concrete material properties as input (e.g., modulus of elasticity, tensile strength) and by fitting creep and shrinkage parameters to experimentally-measured creep and shrinkage strains, respectively. The tension-softening parameter b_{ts} was varied to obtain the best agreement of deflections with each specimen, with values ranging between 0.40 and 0.70. Each beam and slab was modelled using 20 'dispBeamColumn' elements in OpenSees with an approximate length of 200 mm, each discretized into 40 concrete fibres over the cross-section height. For reinforcement, the Steel01 material available in OpenSees was adopted (Mazzoni et al., 2006), which models steel using a bilinear stress–strain relationship with kinematic hardening. Relaxation of the reinforcing bars over time was not modelled since this effect was expected to be negligible at low steel stress levels, typical of non-prestressed beams, under service loads. An example input file for Beam B1a is provided online as Mendeley Data (Tošić et al., 2019b). As shown in Fig. 1, the agreement between the numerical results from TDConcreteMC10NL ('OS') and experimental measurements ('exp.') was excellent, with the time evolution of deflection, *a*, successfully captured.

2.3. Generalized calibration of TDConcreteMC10NL

As described in the previous section, the analysis results in Fig. 1 were generated using measured concrete creep and shrinkage strains as well as a best-fit b_{ts} value for each specimen. The next step in the study was to calibrate a more generalized concrete model suitable for use in a parametric investigation based on the *fib* Model Code 2010 and proposed adjustments for RAC material behaviour. A database of measured deflections from three experimental programs (Knaack and Kurama, 2015b; Seara-Paz et al., 2018; Tošić et al., 2018b) was used for this purpose (Tošić et al., 2019d), including 15 RAC beams and 10 NAC beams loaded in sustained four-point bending. Full details of the materials used in these studies (e.g., RCA composition and water absorption) and characteristics of the tested beams are available in the cited studies. The considered beams were produced with 50% and 100% of coarse RCA (by volume), i.e., the concretes were RAC50 and RAC100.

The reinforcing steel in each specimen was modelled using the Steel01 material in OpenSees and the measured yield strength. For concrete, all material input values were calculated from the measured concrete compressive strength, with adjustments for RAC from Tošić et al. (2019a, 2019d, 2018a) as follows. The modulus of elasticity, E_{cm}, of RAC was calculated as

$$E_{cm} = 21500 \cdot \left(1.0 - 0.3 \cdot \frac{RCA\%}{100}\right) \cdot \left(\frac{f_{cm}}{10}\right)^{1/3} \quad (3)$$

where, $RCA\%$ is the volumetric percentage of coarse NA replacement with coarse RCA, and f_{cm} is the measured RAC compressive strength. Similarly, shrinkage strain and creep coefficient for RAC were adjusted as:

$$\varepsilon_{cs,RAC}(t,t_s) = \left(\frac{RCA\%}{f_{cm}}\right)^{0.30} \cdot \varepsilon_{cs}(t,t_s) \geq \varepsilon_{cs}(t,t_s) \quad (4)$$

$$\varphi_{RAC}(t,t_0) = 1.12 \cdot \left(\frac{RCA\%}{f_{cm}}\right)^{0.15} \cdot \varphi(t,t_0) \geq \varphi(t,t_0) \quad (5)$$

where, $\varepsilon_{cs,RAC}$ is the total RAC shrinkage strain, ε_{cs} is the total shrinkage strain calculated according to the *fib* Model Code 2010, φ_{RAC} is the total RAC creep coefficient, and φ is the total creep coefficient calculated according to the *fib* Model Code 2010.

The concrete tensile strength, f_{ctm}, was calculated using the compressive strength, equally for NAC and RAC, as no significant differences in the relation between the compressive and tensile strengths were observed in literature (Pacheco et al., 2019):

$$f_{ctm} = 0.3 \cdot f_{ck}^{2/3} \quad (6)$$

where, f_{ck} is the characteristic compressive strength of concrete, which was taken as $f_{ck} = f_{cm} - 8$ MPa.

Each specimen was modelled using 20 'dispBeamColumn' elements discretized into 40 concrete fibres over the section depth. Table 1 shows the results for the NAC beams in terms of the 'final' (last measured) deflection. For comparison, predictions are also given using the ζ-method numerical integration of curvatures, as in Tošić et al. (2019d). The TDConcreteMC10NL predictions in Table 1 were obtained using a constant calibrated tension-softening parameter b_{ts} of 0.8. Although this value is higher than the value of 0.4 recommended in Tamai et al. (1988), it is in agreement with Knaack and Kurama (2018) when using the ACI-based TDConcrete model. The reason for such a difference in the value of b_{ts} could lie in the fact that the original model was calibrated on concrete specimens with yielding reinforcing bars under axial tension, whereas its current use in flexural specimens with steel stresses in the linear-elastic range requires a different value. Furthermore, the results of axial tension tests can show strong dependence on the stiffness of the testing apparatus. Nonetheless, the value of 0.8 was considered to provide good and consistent analysis results, considering the statistical descriptors of the predicted-to-measured final deflection ratio, a_{calc}/a_{exp}: the mean values are 0.99 and 0.99, with coefficient of variation (CoV) values of 15.8% and 19.6%, for the ζ-method and

TDConcreteMC10NL, respectively. These results confirm an excellent agreement between the predicted and measured deflections, as well as a near-equal performance in terms of precision and accuracy using TDConcreteMC10NL and the ζ-method.

Similarly, the final measured and TDConcreteMC10NL deflections for the RAC beams are compared in Table 2, together with values using the modified ζ-method for RAC from Tošić et al. (2019d). For optimal predictions, the tension-softening parameter, b_{ts} for the RAC beams was calibrated to a slightly greater value of 0.9, in order to model the weaker tension-stiffening effect in RAC beams. This is consistent with Tošić et al. (2019d), where the empirical coefficient β in the ζ-method is decreased, also simulating weaker tension-stiffening for RAC. In terms of the a_{calc}/a_{exp} ratio, the mean values are 1.01 and 0.94, with CoV values of 20.7% and 28.5%, for the ζ-method and TDConcreteMC10NL, respectively. Although the values for the two methods are not completely equal, the differences are not statistically significantly. Hence, the results are considered as having sufficiently good precision and accuracy in the predictions from both TDConcreteMC10NL and the modified ζ-method for RAC beams.

3. Parametric study on long-term deflections of reinforced RAC elements using OpenSees

After validating and calibrating TDConcreteMC10NL for general use, a parametric study on the long-term deflections of reinforced RAC elements was performed. Since only a limited number of experimental results on the long-term deflections of RAC elements are available, the aim of the study was to assess the implications of RAC SLS design using the proposed modifications of the *fib* Model Code 2010 for RAC, expanding to a wide range of parameters. For this purpose, TDConcreteMC10NL was considered advantageous relative to the ζ-method for two reasons. First, using OpenSees and TDConcreteMC10NL allows easy modelling of any statical system and cross-section shape. Second, TDConcreteMC10NL can provide information on the strain distribution and composition at any point in a member, thus allowing the significance of shrinkage and creep (as well as their basic and drying components) to be separately assessed more easily.

The parametric investigation was conducted using three coarse aggregate replacement amounts as NAC, RAC25, and RAC50, with 0%, 25%, and 50%, respectively, of coarse RCA by volumetric replacement of NA. The 25% replacement ratio was adopted in light of a consensus in the literature that coarse RCA replacements up to 25% (or up to approximately 15% in terms of *total* aggregate replacement ratio) do not affect the properties of RAC relative to companion NAC (Bodet et al., 2018). Note that although the concrete standard EN 206:2013 (CEN, 2013) allows higher RCA replacement ratios (e.g., up to 30% for exposure classes XC1 and XC2), it does not take into account changes in the mechanical properties of concrete from RCA incorporation.

Coarse RCA replacement ratios above 50% were not investigated because: 1) greater replacement utilization of RCA is not considered feasible for widespread application in light of the available supplies of RCA; 2) deterioration in the mechanical properties of RAC (especially for stiffness, creep, and shrinkage) becomes excessive with higher replacement ratios; and 3) previous multi-criteria analyses have shown that RAC50 is an optimal choice considering environmental and economic factors (Tošić et al., 2015). The authors also believe that considering the high uncertainties associated with RCA quality, concretes with coarse RCA incorporation ratios above 50% should be experimentally tested prior to any structural application. As such, the aim of the study was to promote the realistic use of RAC and focusing on positive aspects of lower RCA incorporation ratios up to 50% replacement.

3.1. One-way slabs

3.1.1. Modelling one-way slabs

As a first step in the parametric study, one-way slabs were chosen for two reasons. First, the design of one-way slabs is often governed by deflection considerations. Second, most of the concrete in a structure is used in slabs; hence, the application of RAC in slabs would maximize its benefits. As shown in Fig. 2, two statical systems were considered: a simply supported slab and a continuous slab (modelled as one half of a three-span continuous slab). The slab width was taken as 1000 mm (i.e., 1 m strip of a one-way slab), while the slab height, h, was varied as 200 and 300 mm. Assuming exposure class XC1, the reinforcement centre of gravity, d_1, was taken as 30 mm for NAC and RAC25, but was increased to 35 mm for RAC50 (i.e., concrete cover was increased by 5 mm), consistent with findings on the reduced carbonation resistance of RAC (Carević et al., 2019; Silva et al., 2015). As the aim of the study was to assess the deflections of RAC elements considering design guidelines proposed for practice, the increased cover for RAC50 was considered appropriate. Thus, the effective depth was varied as d = 170 mm (NAC and RAC25) and 165 mm (RAC50) for slabs with h = 200 mm, and 270 mm (NAC and RAC25) and 265 mm (RAC50) for slabs with h = 300 mm. The span length, L, was varied by varying the span-to-effective depth ratio, L/d between 20 and 35 for the simply supported slabs, and between 25 and 40 for the continuous slabs. Note that because of the reduced effective depth for RAC50, these slabs had identical L/d ratios but reduced span length, L as compared with their NAC and RAC25 counterparts. However, since the aim was to assess the maximum deflections of these elements in comparison with allowable deflections given as a function of L, this was considered appropriate.

Two concrete strength classes, C25/30 and C40/50, were considered in order to capture the effect of mechanical properties. The concrete compressive strength was used to calculate the modulus of elasticity, tensile strength, shrinkage strain, and creep coefficient. For both RAC25 and RAC50, the modulus of elasticity, shrinkage strain, and creep coefficient were adjusted using Eqs. (3)–(5). The tension stiffening parameter b_{ts} was set as 0.8 for NAC and RAC25, and as 0.9 for RAC50, following the calibration results in Section 2.3.

Relative humidity (RH) was varied as 50% and 70% to simulate higher and lower shrinkage and creep. When calculating shrinkage and creep, a constant notional size was adopted, equal to the slab thickness (i.e., considering a middle strip of an "infinitely" wide slab). In this way, drying was modelled as uniform across the cross-section height, respecting the applicability of Model Code 2010 creep and shrinkage models. The total factored design load was q_{Ed} = 15 kN/m^2, composed of self-weight, g_{sw} = 5 kN/m^2, additional dead load, Δg = 2.8 kN/m^2, and live load, q = 3 kN/m^2 (the design load was calculated as $q_{Ed} = 1.35 \cdot g_{sw} + 1.35 \cdot \Delta g + 1.50 \cdot q$). These loads were considered as typical for residential buildings (EN 1991-1-1, 2002). For the live load, two values of the ψ_2 coefficient (defining the quasi-permanent portion) were considered as 0.0 and 0.6, which resulted in the quasi-permanent service load-to-factored design load ratio, q_{qp}/q_{Ed}, to be varied as 0.52 and 0.64 to assess the effect of service-load magnitude on the long-term slab deflections.

For each slab span length, L and height, h, the necessary ULS reinforcement $A_{s,ULS}$ was adopted (i.e., no excess reinforcement was considered), checking also for the minimum reinforcement ratio limit of 0.013% (EN 1992-1-1, 2004). For the simply supported slabs, the reinforcement was assumed to be constant along the entire span. For the continuous slabs, the reinforcement over the interior support was adopted over a length of $0.3 \cdot L$ on each side of the support, whereas the reinforcement in the spans was adopted constant over each span. Considering the necessary ULS reinforcement, the reinforcement ratio for the simply supported slab increased from 0.18% for L/d = 20 to 0.58% for L/d = 35. For the continuous slabs, the reinforcement ratio above the support increased from 0.22% for L/d = 25 to 0.61% for L/d = 40; for the end span it ranged from

0.18% for L/d = 25 to 0.48% for L/d = 40; and for the interior span, it remained equal to the minimum reinforcement ratio, i.e., 0.14% for class C25/30 and 0.18% for class C40/50. Reinforcement was modelled using the Steel01 material model in OpenSees, with a yield strength of 500 MPa, modulus of elasticity of 200 GPa, and a hardening modulus of 20 GPa.

Considering eight L/d ratios for each set of parameters, a total of 384 cases were analysed for each of the simply supported and continuous slab configurations. The parameters for all of these cases are provided as an Excel file in the Supporting Information available with the online version of the article. The analyses were performed according to the following service (i.e., unfactored) loading sequence. Moist curing was assumed to end at 7 days (start of shrinkage, no loading); self-weight was applied at 14 days; additional dead load was applied at 60 days; full live load was applied (to cause maximum cracking) at 180 days, and then immediately, part of the live load was removed leaving only the quasi-permanent load on the slab. Each analysis was continued over a total duration of 25 years, which was adopted as a compromise between the longer computation time and the relatively small additional deflections that were expected beyond 25 years (e.g., from 25 to 50 years, deflections were expected to increase less than 3–5%). Therefore, cracking was considered to occur both due to shrinkage (starting at 7 days) and load; in order to model the maximum extent of cracking that can appear in service, the full characteristic load (self-weight + additional dead load + full live load) were applied, followed by a partial unloading of the live load in order to retain only the quasi-permanent load (self weight + additional dead load + part of live load) as the long-term load.

Simply supported and continuous slabs were modelled using 20 and 30 'dispBeamColumn' elements, respectively (i.e., the continuous slab models included 10 additional elements over the half-length center span), discretized into 40 concrete fibres over the section height. At the start of shrinkage (7 days), the global variable "setCreep" was set to 1 in order to begin accumulating shrinkage strains. Subsequently, at each loading step (14, 60, and 180 days), a Static Analysis was performed first for the initial application of the intended load, followed by a time-dependent analysis in order to accumulate creep and shrinkage deformations until the next loading age or end of analysis. In each time-dependent analysis, the time steps were logarithmically spaced to accurately model the greater strain increments immediately after the application of load. The entire parametric study was automated and ran with MATLAB (Simulink). For both the load application in Static Analysis and time-dependent analysis, the nonlinear solution algorithm was programmed to switch between the Newton, Modified Newton, and Newton Line Search methods (Mazzoni et al., 2006) to achieve convergence.

3.1.2. Results for one-way slabs

In order to assess the differences in the slab deflections, the analysis results were plotted in terms of the final deflection to limit deflection ratio, a/a_{lim}—where, a_{lim} was taken as $L/250$ (FIB, 2013)— versus the L/d ratio. The a/a_{lim} versus L/d results for all of the simply supported and continuous slab parameter sets are plotted as Figs. S1–S4 in the Supporting Information available with the online version of the article. Looking at the simply supported slabs first, selected results are shown in Fig. 3 for h = 200 mm and $q_{\mathrm{qp}}/q_{\mathrm{Ed}}$, = 0.52, with varying concrete class (i.e., concrete strength) and RH. It can be seen that the a/a_{lim} ratio starts well below 1.0 because, for lower values of L/d (ranging between 20–26), the slabs are uncracked or very close to the cracking load. With increasing L/d ratio, a/a_{lim} quickly rises above 1.0 up to values close to 3, signifying that if exactly the ULS-reinforcement is adopted (i.e., no excess reinforcement), the deflection limit can be greatly surpassed.

Importantly, it can be seen from Fig. 3 (and Figs. S1–S2 in the Supporting Information) that NAC and RAC25 have practically identical a/a_{lim} ratios. This is expected and also in line with research findings that there are no significant differences between NAC and RAC for coarse aggregate replacement ratios up to 20–25% (i.e., decrease in modulus of elasticity and increases in creep and shrinkage are insignificant for RAC25). The increases in a/a_{lim} ratios for RAC50 are more visible, but usually within 5–10%, with the largest differences for concrete class C25/50, RH = 50%, and $q_{\mathrm{qp}}/q_{\mathrm{Ed}}$ = 0.52. Overall, the concrete class has the largest influence on the deflection increases caused by the use of RAC50, whereas the other parameters (h, RH, $q_{\mathrm{qp}}/q_{\mathrm{Edh}}$) affect the deflections of NAC and RAC50 slabs by nearly equal amounts.

The effects of the individual parameters are further investigated in Fig. 4, focusing on RAC50. Again, the strong effect of the concrete class can be seen in each case: the increase of concrete strength from C25/30 to C40/50 reduces the a/a_{lim} ratio by approximately 25%. Note that since all mechanical and time-dependent properties of concrete were determined from the compressive strength, this effect is a superposition of the separate effects from changes in modulus of elasticity, tensile strength, shrinkage, and creep between classes C40/50 and C25/30. The increase of $q_{\mathrm{qp}}/q_{\mathrm{Ed}}$ from 0.52 to 0.64 increases the a/a_{lim} ratio by approximately 15–

20%. The increase of RH from 50% to 70% leads to a reduction of $a/a_{\lim}$ by approximately 15%. The slab height, h causes no significant changes in the $a/a_{\lim}$ ratio.

In order to further investigate the results, the capability of OpenSees to provide the strain components as output, as in Eq. (2), was used. For example, Figure 5 presents the time evolution of the creep, shrinkage, mechanical, and total strains of the top fibre in the mid-span cross-section of the simply supported one-way slabs for the case of $L/d = 20$, $RH = 50\%$ and $q_{qp}/q_{Ed} = 0.52$. It can be seen that the shrinkage strain is by far the largest component, making up 77–83% of the total strain, whereas the mechanical and creep strains comprise 5–6% and 10–16%, respectively. The reason for this is the fact that for $L/d = 20$ the slab is uncracked; hence, the mechanical and creep strains are very small. As such, in this case, the main influence on curvature, and consequently, deflections comes from shrinkage. By comparing the left and right graphs in Fig. 5, the effect of RCA can be seen (albeit for RAC50 slabs with shorter span lengths, L): for concrete C25/30, the RAC50 maximum shrinkage strain is 0.90‰, compared with 0.79‰ for NAC (13.9% increase); however, for concrete C40/50, the maximum shrinkage strains are 0.71‰ and 0.70‰ for RAC50 and NAC, respectively (only 1.4% increase). This increase in RAC shrinkage strains can be seen through the RAC shrinkage adjustment factor in Eq. (4). The effect of the RAC creep adjustment factor from Eq. (5) on the creep strains can also be seen. As for the mechanical strains, they are approximately 10% larger in the case of RAC50 due to the lower modulus of elasticity presented in Eq. (3).

A similar analysis is presented in Fig. 6 for the case of $L/d = 35$ ($RH = 50\%$ and $q_{qp}/q_{Ed} = 0.52$). In this case, the slab is heavily cracked; therefore, mechanical strains are much higher than those in Fig. 5, and consequently, creep strains are also higher. The resulting contributions from shrinkage, creep, and mechanical strains (43–49%, 32–42%, and 14–19% respectively) are more consistent, keeping in mind that the shrinkage strains in Figs. 5 and 6 are the same since they are not load dependent. Again, the effect of increased shrinkage and creep strains when using RAC50 can be seen by comparing the left and right graphs in Fig. 6. Additionally, the decreasing differences between NAC and RAC50 when using a higher concrete class can be seen between the upper and lower graphs. The results in Figs. 5 and 6 can provide guidance on when it may be appropriate (in terms of the L/d ratio, RCA volume, and concrete class) to implement shrinkage-reducing and creep-reducing measures, such as prolonged curing, delayed loading, or admixtures. For example, implementing only shrinkage-reducing measures may be more meaningful for lower L/d ratios, while, for higher L/d ratios, it would be also beneficial to implement creep-reducing measures, such as delayed formwork removal.

Looking back at Fig. 3 and the additional cases in Figs. S1–S2 in the Supporting Information, it can be seen that the deflections of simply supported one-way slabs with RAC50 satisfy the allowable limit (i.e., $a/a_{\text{lim}} < 1$) for a wide range of L/d ratios, depending on the parameters. Generally, for concrete C25/30, L/d should be less than about 22, whereas for concrete C40/50, this limit can be increased to 29. This result also agrees with limit L/d ratios suggested for one-way simply supported slabs in design codes (EN 1992-1-1, 2004), especially considering that in these analyses, no excess reinforcement was used above the ULS-required areas. This further supports the applicability of RAC50 slabs for typical L/d ratios, since despite the increases, the deflections are still within limits for most typical cases.

Similarly, the results for continuous slabs are presented in Fig. 7 and Figs. S3–S4 in the Supporting Information. The conclusions reached for simply supported slabs are still applicable, with increased L/d limits. Again, NAC and RAC25 are practically identical, and the concrete class has the largest influence on the deflection increases caused by the use of RAC50, whereas the other parameters (h, RH, $q_{\text{qp}}/q_{\text{Edh}}$) affect the deflections of NAC and RAC50 slabs by nearly equal amounts. The deflection increases for RAC50 are within 5–10% and are largest for concrete class C25/50, $RH = 50\%$, and $q_{\text{qp}}/q_{\text{Ed}} = 0.52$. Similar to Fig. 4, Fig. 8 presents the effects of individual parameters for RAC50. In this case, the change from C25/30 to C40/50 reduces the a/a_{lim} ratio by 25–30%, which is somewhat greater than for simply supported slabs. The increase of $q_{\text{qp}}/q_{\text{Ed}}$ from 0.52 to 0.64 increases the a/a_{lim} ratio by approximately 15–25%. As for simply supported slabs, the increase of RH from 50% to 70% leads to a reduction of a/a_{lim} by approximately 15%. Importantly, for continuous slabs, the maximum L/d ratios that satisfy the deflection limits are increased to approximately 28 for concrete C25/30, and 36 for C40/50.

3.2. T-beams

3.2.1. Modelling of T-beams

A parametric study was performed on T-beams as well, investigating another typical element type in reinforced concrete structures. In this case, only simply supported boundary conditions were considered. This is because, as will be shown later, deflection control was found to be not critical in simply supported T-beams, and by extension, it is less important in continuous beams. The beam height, h, was varied as 500 or 700 mm, and the corresponding flange height, h_f, was varied as 150 and 200 mm, respectively. The web width, b_w, and effective flange width, b_{eff}, were kept constant as 250 mm and 2000 mm, respectively.

The loads on the T-beams were the same as for slabs (15 kN/m^2), but with a tributary width of 6 m rather than 1 m, resulting in a factored design load of q_{Ed} = 90 kN/m. The concrete classes of C25/30 and C40/50, *RH* of 50% and 70%, and q_{qp}/q_{Ed} of 0.52 and 0.64 were also the same as those for the slab analyses. The tensile reinforcement was adopted as the areas required by ULS design, constant across the span, with an additional 2Ø16 bars (402 mm^2) of compressive reinforcement (slab reinforcement was not considered in the beam analyses). Hence, the tensile reinforcement ratio (determined in relation to b_{eff}) for the beams increased from 0.13% for L/d = 8 to 0.57% for L/d = 20. The centroid of the reinforcement was modelled at 50 mm for NAC and RAC25, and 55 mm for RAC50 (i.e., 5 mm greater cover for RAC50, like in the slab analyses). The span-to-effective depth, L/d ratios were analysed in increments of 2 from 8 to 20. The loading sequence, modelling, and analysis approach for the beams were the same as those for the slabs.

3.2.2. Results for T-beams

Selected results are shown in Fig. 9, with complete results presented as Figs. S5–S6 in the Supporting Information accompanying this article. The general trends for the beams are the same as for slabs; however, with somewhat decreased effects from RCA. The effects of all parameters for RAC50 are shown in Fig. 10. As in the case of slabs, increased concrete class, decreased q_{qp}/q_{Ed}, and increased humidity all cause decreased a/a_{lim} ratios. Most importantly, the L/d limit—above which deflection control is not satisfied—is about 12. This is an L/d ratio that is almost always satisfied for T-beams in residential construction (EN 1992-1-1, 2004); therefore, it can be concluded that deflection control is not an issue for T-beams in practice, whether they are NAC or RAC.

4. Implications for SLS design of reinforced RAC elements

The parametric analysis results presented in this study have important implications for the SLS design and applicability of RAC in reinforced concrete elements, particularly for slabs and T-beams. It is shown that both slab and beam elements with RCA percentages up to 25% can be designed just like NAC structures, with no modifications or span restrictions needed to limit deflections. In the case of T-beams, RCA contents up to 50% are also possible with no practical implications from deflection control. The increase in deflection is greatest for RAC50 slabs. This means that for the same height, shorter spans can be achieved with RAC50, limited to L/d ratios of about 20-25 and 27-32 (depending on the concrete class) for simply-supported and continuous slabs, respectively. Despite the span limitations, these results can further promote the use of RCA, especially considering the environmental and economic benefits of RAC50 (Tošić et al., 2015).

Recall that the deflection results in this paper are for models where only the ULS-required reinforcement was assumed. Increased tensile (and compressive) steel areas, as is likely in practice, can improve the behaviour of RAC elements. This was considered for the worst case scenario (i.e., when deflection increases for RAC50 from NAC were the largest) for both simply-supported and continuous slabs with C25/30, RH50%, and $q_{qp}/q_{Ed} = 0.52$. To make meaningful comparisons, the spans of the NAC and RAC50 slabs were taken equal (i.e., RAC50 had a 5-mm smaller effective depth, thus requiring a greater area of reinforcement).

In this worst-case scenario, the a/a_{lim} ratios for RAC50 were 20% higher than for NAC. For the maximum deflections of the RAC50 slabs to be comparable to NAC, it was necessary to: 1) increase the tensile reinforcement areas by 25% and 15% for h = 200 and 300 mm, respectively; and 2) at the same time, use compressive reinforcement areas of 50% of the tensile reinforcement areas. While this is not an insignificant increase of reinforcement (in total, 80%), the required increases in steel areas would be smaller for other cases, or not even necessary for the majority of cases with concrete class C40/50. This may be a plausible way to allow the use of RAC50 in longer spans, without increasing the element height, h.

5. Conclusions

In this study, an open-source numerical concrete material model is described for the simulation of time-dependent behaviour of reinforced concrete elements. Different from a previously-developed concrete material, the new model includes nonlinear behaviour of concrete in compression and utilizes the *fib* Model Code 2010 for shrinkage and creep strains. The model was first validated by successfully reproducing measured long-term slab and beam deflection curves using measured material properties, including creep and shrinkage strains, for input. Then, the model was calibrated for general application using proposed adjustment factors for RAC stiffness, creep, and shrinkage (rather than measured values) on a database of RAC and NAC beams. This calibration study also resulted in the quantification of the reduced tension-stiffening effect of RAC.

By carrying out a comprehensive parametric study on NAC and RAC one-way slabs and T-beams using this model, and by considering relevant influencing parameters, the following conclusions were drawn:

- For both beams and slabs, and all parameter values investigated, the behaviour of RAC25 is nearly identical to that of NAC, thus requiring no application limitations when using RAC25. This is a strong argument in favour of using RCA in lower replacement amounts (less than 25%) in structural applications.
- For both beams and slabs, RAC50 can cause considerable increases in deflections as compared with NAC and RAC25. However, these increases are pronounced only in the case of low compressive strength (i.e., class C25/30), and they are greatly reduced when using a higher compressive strength (C40/50).
- Overall, the concrete class (strength) has the largest influence on the deflection increases caused by the use of RAC50, whereas the other parameters (h, RH, $q_{\mathrm{qp}}/q_{\mathrm{Edh}}$) affect the deflections of NAC and RAC50 elements by nearly equal amounts.
- In the case of simply supported one-way RAC50 slabs, the limiting L/d ratio for satisfying allowable deflections is in the range of 22–29, depending on the concrete class. For continuous one-way slabs, this ratio is in the range of 28–36, and for simply supported T-beams, it is in the range of 12–16. RAC50 can be used for L/d ratios lower than these values since deflections are satisfied for all concrete types.
- For larger L/d ratios and the most unfavourable set of parameter values, it is possible to reduce RAC deflections to levels comparable to NAC by adopting more tensile reinforcement (by about 15–25%) and compressive reinforcement equal to 50% of tensile reinforcement. For more favourable cases, the necessary reinforcement increases are lower or not necessary at all.

The results of this study significantly expand the current knowledge on the deflection behaviour of reinforced RAC members and present an in-depth analysis of the implications of current SLS design proposals for RAC. While the conclusions of this study may be limited to the values of parameters considered herein, the results can provide a strong impetus for the further promotion of RAC use in structural applications.

Acknowledgements

This research was funded by the United States Department of State through a Fulbright Visiting Scholar Grant for the project “Optimization of Stratified Recycled Concrete Structures Based on Numerical Analyses and Life Cycle Assessment.” This support is gratefully acknowledged. The authors also express their gratitude for research assistance provided by Dr. Adam Knaack (Schaefer-Inc) and Dr. Seyed Alireza Jalali (Civil Soft

Science). Any opinions, findings, conclusions, and/or recommendations in the paper are those of the authors and do not necessarily represent the views of the individuals or organizations acknowledged.

Notation

$\varepsilon_{\mathrm{cbc}}$	concrete basic creep strain
$\varepsilon_{\mathrm{cbs}}$	concrete basic shrinkage strain
$\varepsilon_{\mathrm{cdc}}$	concrete drying creep strain
$\varepsilon_{\mathrm{cds}}$	concrete drying shrinkage strain
$\varepsilon_{\mathrm{cs}}$	total concrete shrinkage strain
$\varepsilon_{\mathrm{cs,RAC}}$	total RAC shrinkage strain
φ	total concrete creep coefficient
φ_{RAC}	total RAC creep coefficient
$\varepsilon_{\mathrm{ct,m}}$	concrete tensile strain at cracking
ε_{m}	concrete mechanical strain
$\varepsilon_{\mathrm{tot}}$	concrete total strain
ρ_{l}	tensile reinforcement ratio
σ_{ct}	concrete tensile stress
a	deflection
a_{calc}	calculated deflection
a_{exp}	measured deflection
a_{lim}	deflection limit
Δg	additional dead load
b	width
b_{eff}	effective flange width
b_{ts}	tension-softening parameter
b_{w}	web width
d	effective depth
f_{ck}	characteristic concrete compressive strength
f_{cm}	mean concrete compressive strength

f_{ctm} mean concrete tensile strength

g_{sw} self-weight

h height

h_f flange height

q live load

q_{qp} quasi-permanent load

q_{Ed} design load

t time

t_0 concrete age at loading

t_s concrete age at start of drying

$A_{s,ULS}$ ULS-required reinforcement

E_{cm} concrete modulus of elasticity

L span length

$RCA\%$ percentage replacement of coarse NA with RCA

RH relative humidity

References

ACI 209R-92, 1992. Prediction of Creep, Shrinkage, and Temperature Effects in Concrete Structures. American Concrete Institute, Farmington Hills, MI.

Azúa, G., González, M., Arroyo, P., Kurama, Y., 2019. Recycled coarse aggregates from precast plant and building demolitions: Environmental and economic modeling through stochastic simulations. J. Clean. Prod. doi:10.1016/j.jclepro.2018.11.049

Bodet, R., Colina, H., De Larrard, F., Delaporte, B., Ghorbel, E., Mansoutre, S., Roudier, J., 2018. Comment recycler le béton dans le béton: Recommendations du projet national Recybeton.

Brandes, M.R., Kurama, Y.C., 2018a. Behavior of shear-critical prestressed concrete beams with recycled concrete aggregates under ultimate loads. Eng. Struct. 165, 237–246. doi:10.1016/j.engstruct.2018.03.029

Brandes, M.R., Kurama, Y.C., 2018b. Service-load behavior of precast/prestressed concrete beams with recycled concrete aggregates. ACI Struct. J. doi:10.14359/51702133

Carević, V., Ignjatović, I., Dragaš, J., 2019. Model for practical carbonation depth prediction for high volume fly ash concrete and recycled aggregate concrete. Constr. Build. Mater. doi:10.1016/j.conbuildmat.2019.03.267

CEN, 2013. EN 206: 2013 Concrete - Specification, performance, production and conformity. Brussels.

EN 1991-1-1, 2002. Eurocode 1: Actions on structures - Part 1-1: General actions - Densities, self-weight, imposed loads for buildings. Eurocode 1. doi:ICS 91.010.30; 93.040

EN 1992-1-1, 2004. Eurocode 2: Design of concrete structures - Part 1-1: General rules and rules for buildings. CEN, Brussels.

Fathifazl, G., Razaqpur, A.G., Burkan Isgor, O., Abbas, A., Fournier, B., Foo, S., 2010. Shear strength of reinforced concrete beams with stirrups. Mag. Concr. Res. 62, 685–699. doi:10.1617/s11527-007-9223-3

FIB, 2013. fib Model Code for Concrete Structures 2010. International Federation for Structural Concrete (fib), Lausanne. doi:10.1002/9783433604090

Fisher, C., Werge, M., 2011. EU as a Recycling Society [WWW Document]. ETC/SCP Work. Pap. 2. URL scp.eionet.europa.eu/wp/ETCSCP 2per2011 (accessed 7.7.16).

Gilbert, R.I., Nejadi, S., 2004. An experimental study of flexural cracking in reinforced concrete members under sustained loads. Kensington.

Ignjatović, I., 2013. Ultimate strength of reinforced recycled concrete beams. University of Belgrade.

Knaack, A.M., 2013. Sustainable concrete structures using recycled concrete aggregate: short-term and long-term behavior considering material variability. University of Notre Dame.

Knaack, A.M., Kurama, Y.C., 2018. Modeling Time-Dependent Deformations: Application for Reinforced Concrete Beams with Recycled Concrete Aggregates. ACI Struct. J. 115, 175–190. doi:10.14359/51701153

Knaack, A.M., Kurama, Y.C., 2015a. Creep and Shrinkage of Normal-Strength Concrete with Recycled Concrete Aggregates. ACI Mater. J. 115, 451–462.

Knaack, A.M., Kurama, Y.C., 2015b. Sustained Service Load Behavior of Concrete Beams with Recycled Concrete Aggregates. ACI Struct. J. 112, 565–578. doi:10.14359/51687799

Knaack, A.M., Kurama, Y.C., 2014. Behavior of Reinforced Concrete Beams with Recycled Concrete Coarse Aggregates. ASCE J. Struct. Eng. 141, 1–12. doi:10.1061/(ASCE)ST.1943-541X.0001118.

Li, X., 2009. Recycling and reuse of waste concrete in China. Part I. Material behaviour of recycled aggregate concrete. Resour. Conserv. Recycl. 53, 107–112. doi:10.1016/j.resconrec.2008.11.005

Lye, C.Q., Dhir, R.K., Ghataora, G.S., Li, H., 2016a. Creep strain of recycled aggregate concrete. Constr. Build. Mater. 102, 244–259. doi:10.1016/j.conbuildmat.2015.10.181

Lye, C.Q., Ghataora, G.S., Dhir, R.K., 2016b. Shrinkage of recycled aggregate concrete, in: Structures and Buildings, Proceedings of the Institution of Civil Engineers. ICE, pp. 1–25. doi:10.1680/jstbu.15.00138

Mazzoni, S., McKenna, F., Scott, M.H., Fenves, G.L., 2006. OpenSees command language manual. Pacific Earthq. Eng. Res. Cent.

McKenna, F., 2011. OpenSees: A framework for earthquake engineering simulation. Comput. Sci. Eng. doi:10.1109/MCSE.2011.66

Mohd-Yassin, M.H., Filippou, F.C., 1994. Nonlinear analysis of prestressed concrete structures, in: Structures Congress XII.

Nixon, P.J., 1978. Recycled concrete as an aggregate for concrete - a review. Mater. Struct. 11, 371–378.

Pacheco, J., Brito, J. De, Soares, D., 2015. Destructive Horizontal Load Tests of Full-scale Recycled Aggregate Concrete Structures. ACI Struct. J. 112, 815–826.

Pacheco, J., de Brito, J., Chastre, C., Evangelista, L., 2019. Experimental investigation on the variability of the main mechanical properties of concrete produced with coarse recycled concrete aggregates. Constr. Build. Mater. doi:10.1016/j.conbuildmat.2018.12.200

PT1prEN1992-1-1, 2017. Eurocode 2: Design of concrete structures – Part 1-1: General rules, rules for buildings, bridges and civil engineering structures. CEN, Brussels.

Santana Rangel, C., Amario, M., Pepe, M., Yao, Y., Mobasher, B., Toledo Filho, R.D., 2017. Tension stiffening approach for interface characterization in recycled aggregate concrete. Cem. Concr. Compos. 82, 176–189. doi:10.1016/j.cemconcomp.2017.06.009

Seara-Paz, S., González-Fonteboa, B., Martínez-Abella, F., Carro-Lopez, D., 2018. Long-term flexural performance of reinforced concrete beams with recycled coarse aggregates. Constr. Build. Mater. 176, 593–607.

Silva, R.V., 2015. Use of recycled aggregates from construction and demolition waste in the production of structural concrete. Universidade de Lisboa.

Silva, R.V., de Brito, J., Dhir, R.K., 2016. Establishing a relationship between the modulus of elasticity and compressive strength of recycled aggregate concrete. J. Clean. Prod. 112, 2171–2186. doi:10.1016/j.jclepro.2015.10.064

Silva, R.V., Neves, R., de Brito, J., Dhir, R.K., 2015. Carbonation behaviour of recycled aggregate concrete. Cem. Concr. Compos. 62, 22–32. doi:10.1016/j.cemconcomp.2015.04.017

Tam, V.W.Y., Soomro, M., Evangelista, A.C.J., 2018. A review of recycled aggregate in concrete applications (2000-2017). Constr. Build. Mater. 172, 272–292. doi:10.1016/j.conbuildmat.2018.03.240

Tamai, S., Shima, H., Izumo, J., Okamura, H., 1988. Average stress-strain relationship in post yield range of steel bar in concrete. Concr. Libr. JSCE 11, 117–129.

Tošić, N., de la Fuente, A., Marinković, S., 2019a. Creep of recycled aggregate concrete: Experimental database and creep prediction model according to the fib Model Code 2010. Constr. Build. Mater. 195, 590–599. doi:10.1016/j.conbuildmat.2018.11.048

Tošić, N., de la Fuente, A., Marinković, S., 2018a. Shrinkage of recycled aggregate concrete: experimental database and application of fib Model Code 2010. Mater. Struct. Constr. doi:10.1617/s11527-018-1258-0

Tošić, N., Knaack, A., Kurama, Y., 2019b. Supporting documentation for time-dependent concrete material models in OpenSees [WWW Document]. Mendeley Data, v3. doi:10.17632/z4gxnhchky.3

Tošić, N., Knaack, A., Kurama, Y., 2019c. Source code for OpenSees time-dependent concrete material models [WWW Document]. GitHub. URL https://github.com/ntosic87/OpenSees (accessed 12.23.19).

Tošić, N., Marinković, S., Dašić, T., Stanić, M., 2015. Multicriteria optimization of natural and recycled aggregate concrete for structural use. J. Clean. Prod. 87, 766–776.

Tošić, N., Marinković, S., de Brito, J., 2019d. Deflection control for reinforced recycled aggregate concrete beams : Experimental database and extension of the fib Model Code 2010 model. Struct. Concr. 1–15. doi:10.1002/suco.201900035

Tošić, N., Marinković, S., Ignjatović, I., 2016. A database on flexural and shear strength of reinforced recycled aggregate concrete beams and comparison to Eurocode 2 predictions. Constr. Build. Mater. 127, 932–944.

Tošić, N., Marinković, S., Pecić, N., Ignjatović, I., Dragaš, J., 2018b. Long-term behaviour of reinforced beams made with natural or recycled aggregate concrete and high-volume fly ash concrete. Constr. Build. Mater. 176, 344–358.

WBCSD, 2009. The Cement Sustainability Initiative [WWW Document]. World Bus. Counc. Sustain. Dev. URL http://www.wbcsdcement.org/pdf/CSIRecyclingConcrete-FullReport.pdf (accessed 7.7.16).

Xiao, J., Wang, C.Q., Li, J., Tawana, M., 2012. Shake-table model tests on recycled aggregate concrete frame structure. ACI Struct. J. 109, 777–786.

List of figures:

List of tables:

Table 1. Prediction of NAC beam deflections using the OpenSees model and ζ-method

Study	Beam	$b/h/L$ (mm)	ρ_l (%)	f_{cm} (t_0) (MPa)	$t–t_0$ (days)	a_{exp} (mm)	a_ζ (mm)	a_{OS} (mm)
(Tošić et al., 2018b)	NAC7	160/200/3200	0.58	25.0	450	18.94	22.67	22.41
	NAC28			30.5		16.51	18.63	19.40
(Knaack and Kurama, 2015b)	UT-0-28	150/230/3700	1.32	32.6	119	5.00	5.69	6.45
	UT-0-7			39.2		4.62	4.96	4.62
	UC-0-28			49.3		3.51	2.74	2.52
	UC-0-7			32.7		5.11	4.75	4.52
	CC-0-28			40.2		10.19	9.10	9.05
	CC-0-7			36.2		10.69	9.77	9.29
(Seara-Paz et al., 2018)	H50-0	200/300/3400	0.81	63.0	1000	18.39	13.68	13.90
	H65-0		0.86	48.7		11.58	12.19	12.69

Note: a_ζ – deflection using the ζ-method; a_{OS} – deflection using the OpenSees model

Table 2. Prediction of RAC beam deflections using the OpenSees model and ζ-method

Study	Beam	*RCA* (%)	$b/h/L$ (mm)	ρ_l (%)	f_{cm} (t_0) (MPa)	t–t_0 (days)	a_{exp} (mm)	a_ζ (mm)	a_{OS} (mm)
(Tošić et al., 2018b)	RAC28	100	160/200/3200	0.58	28.1	450	14.69	23.42	23.61
(Knaack and Kurama, 2015b)	UT-50-28	50	150/230/3700	1.32	43.6	119	5.38	5.80	4.82
	UT-50-7	50			40.2		6.96	7.89	6.76
	UC-50-28	50			49.6		4.70	4.20	2.84
	UC-50-7	50			43.6		5.99	5.86	4.34
	UT-100-28	100			41.4		7.39	6.71	6.83
	UC-100-28	100			48.2		5.94	5.04	3.68
	UC-100-7	100			40.6		7.62	7.05	5.70
	CC-50-7	50			40.0		12.90	11.05	10.68
	CC-100-28	100			43.8		12.27	11.22	10.31
	CC-100-7	100			38.5		14.68	13.12	12.48
(Seara-Paz et al., 2018)	H50-50	50	200/300/3400	0.81	51.8	1000	14.08	11.37	10.64
	H50-100	100			42.9		15.20	14.57	14.19
	H65-50	50		0.86	42.2		9.63	11.16	10.69
	H-65-100	100			32.4		11.34	14.82	14.87

Note: a_ζ – deflection using the ζ-method; a_{OS} – deflection using the OpenSees model

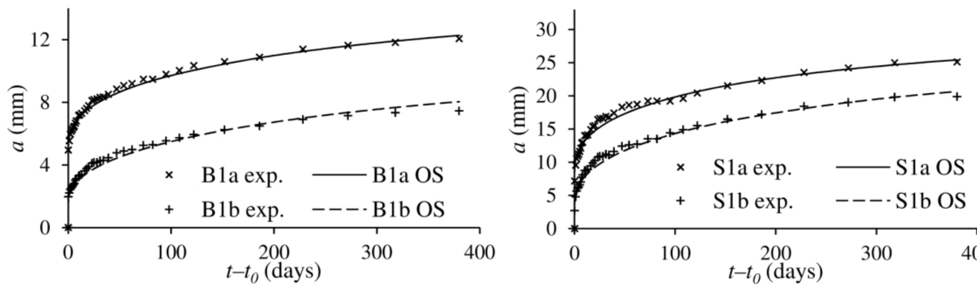

Figure 1. Comparison of measured deflections from Gilbert and Nejadi (2004) with calculated deflections using the OpenSees model

160x45mm (300 x 300 DPI)

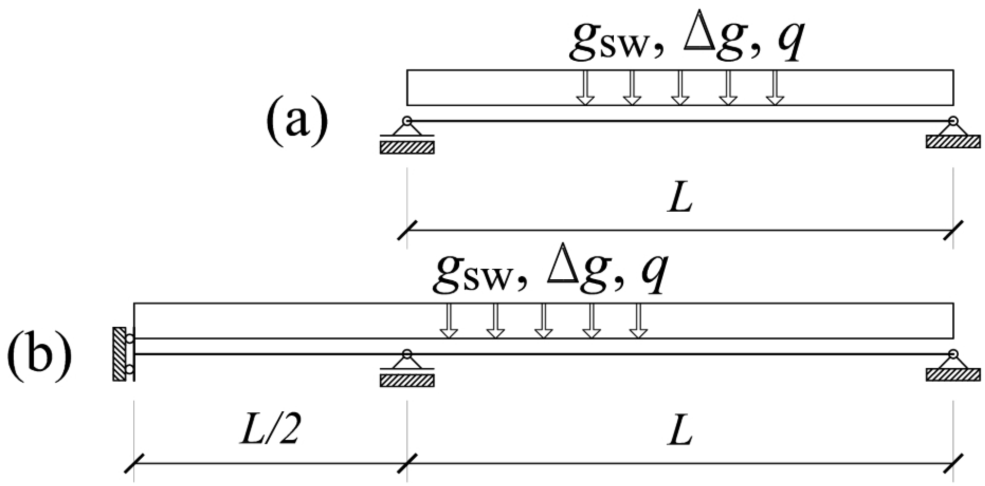

Figure 2. Statical systems of the one-way slabs considered in the parametric study

80x41mm (300 x 300 DPI)

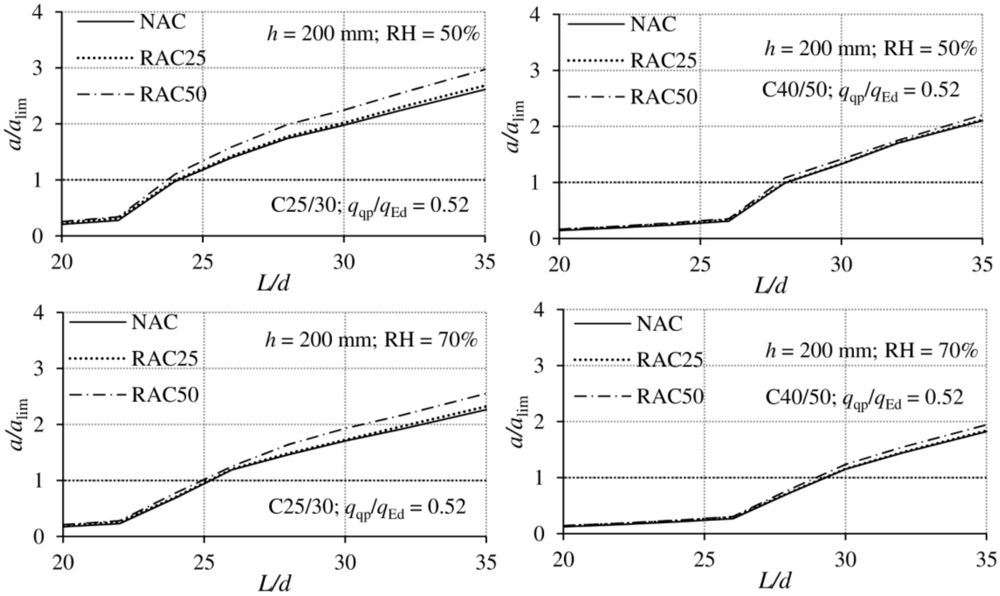

Selected comparisons of a/a_{lim} versus L/d ratio for simply supported slabs with NAC, RAC25, and RAC50

160x96mm (300 x 300 DPI)

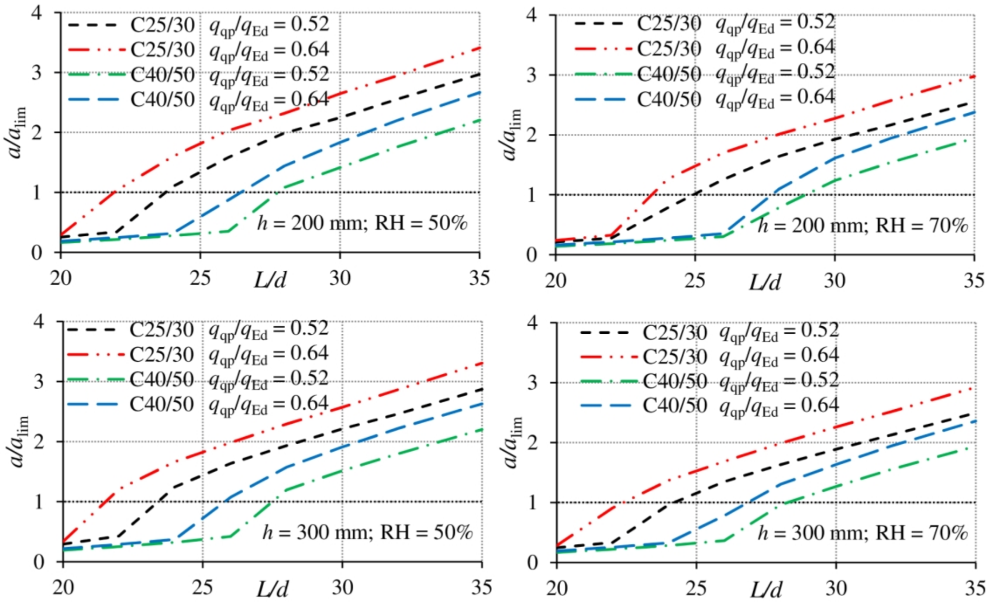

Figure 4. Effects of individual parameters on the a/a_{lim} ratio of simply supported RAC50 slabs

160x96mm (300 x 300 DPI)

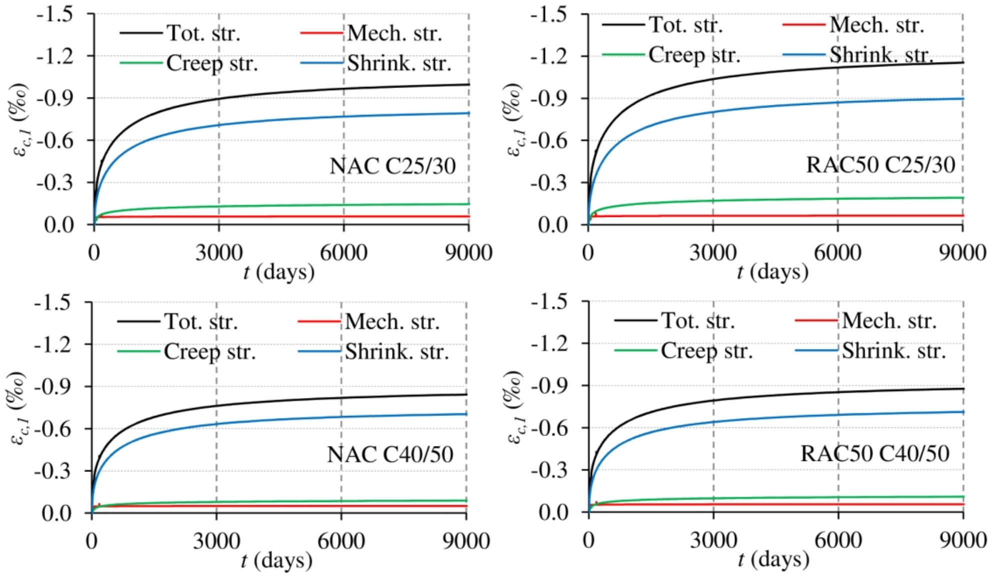

Figure 5. Mid-span top fibre strains for simply supported NAC and RAC50 slabs (L/d = 20, h = 200 mm, RH = 50%, q_{qp}/q_{Ed} = 0.52)

160x93mm (300 x 300 DPI)

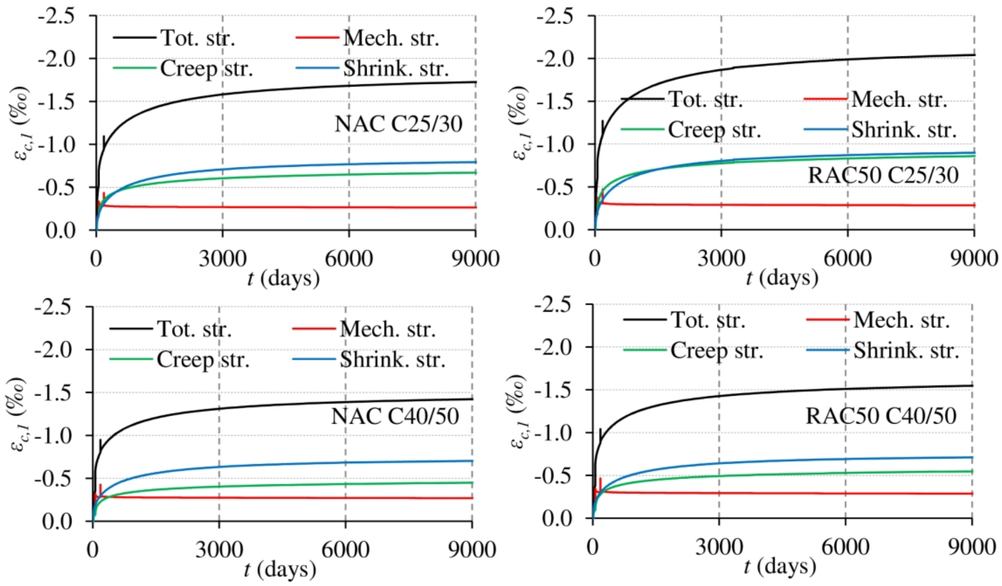

Figure 6. Mid-span top fibre strains for simply supported NAC and RAC50 slabs (L/d = 35, h = 200 mm, RH = 50%, q_{qp}/q_{Ed} = 0.52)

160x93mm (300 x 300 DPI)

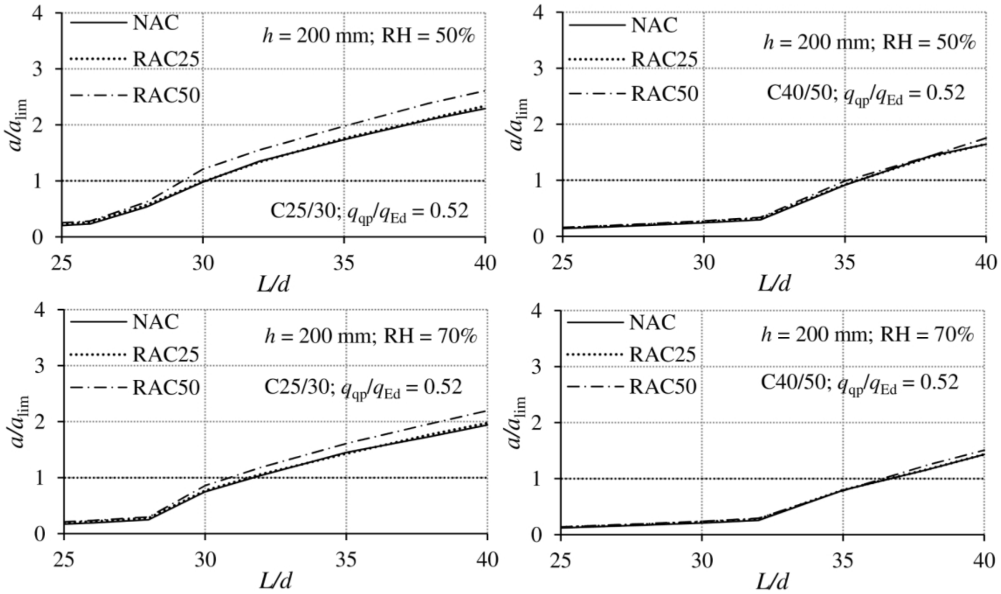

Figure 7. Selected comparisons of a/a_{lim} versus L/d ratio for continuous slabs with NAC, RAC25, and RAC50

160x96mm (300 x 300 DPI)

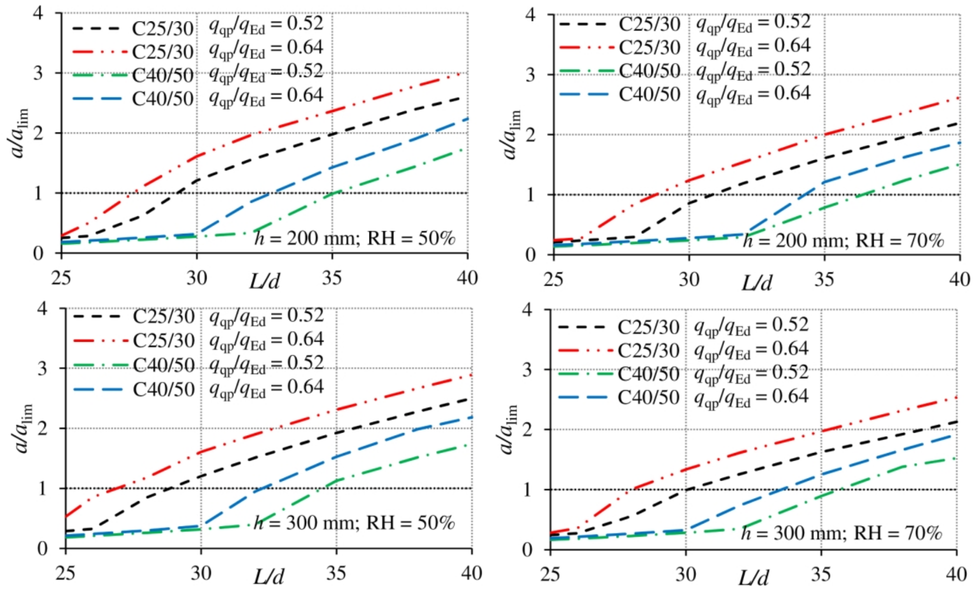

Figure 8. Effects of individual parameters on the a/a_{lim} ratio of continuous RAC50 slabs

160x95mm (300 x 300 DPI)

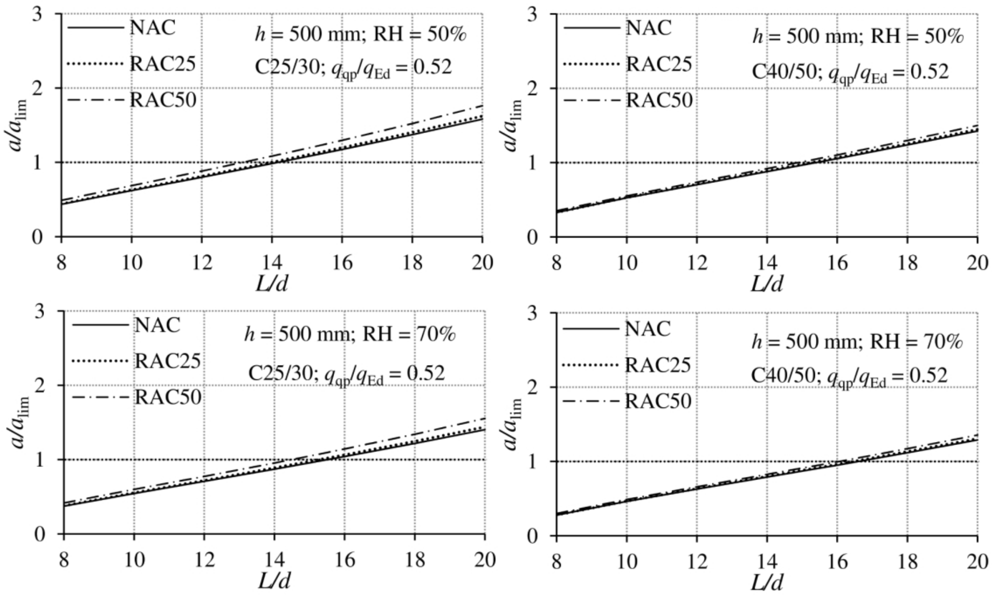

Figure 9. Selected comparisons of a/a_{lim} versus L/d ratio for simply supported T-beams with NAC, RAC25, and RAC50

160x96mm (300 x 300 DPI)

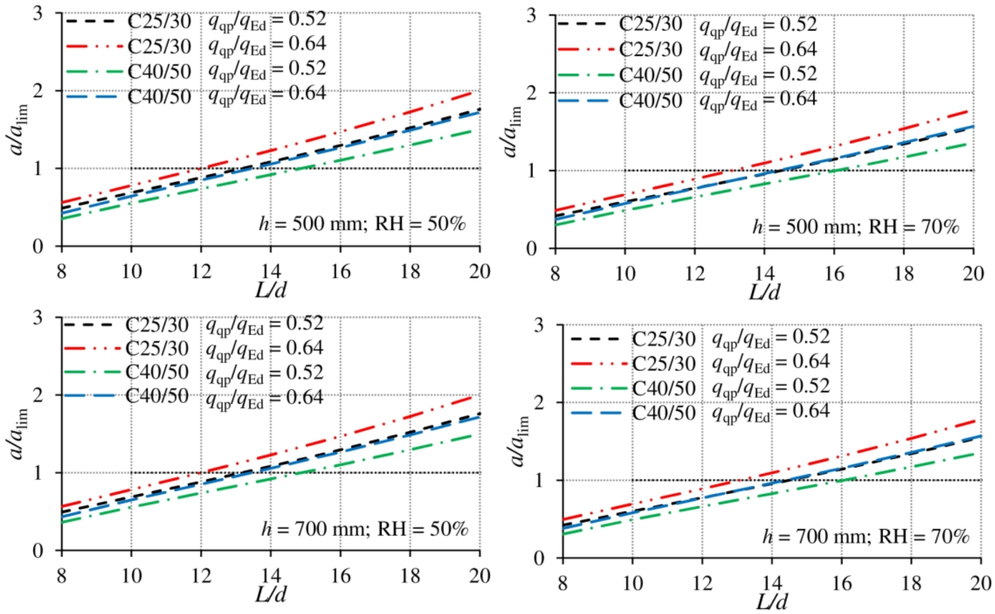

Effects of individual parameters on the a/a_{lim} ratio of simply supported RAC50 T-beams

160x98mm (300 x 300 DPI)

SUPPORTING INFORMATION FOR TECHNICAL PAPER:

Parametric numerical study on deflections of reinforced recycled aggregate concrete slabs and beams based on the *fib* Model Code 2010

Nikola Tošić[a,*], Yahya Kurama[b]

[a] *University of Belgrade, Faculty of Civil Engineering, Bulevar kralja Aleksandra 73, 11000 Belgrade, Serbia*

[b] *Department of Civil and Environmental Engineering and Earth Sciences, University of Notre Dame, Notre Dame, IN, USA*

* Corresponding author:.
E-mail address: ntosic@imk.grf.bg.ac.rs

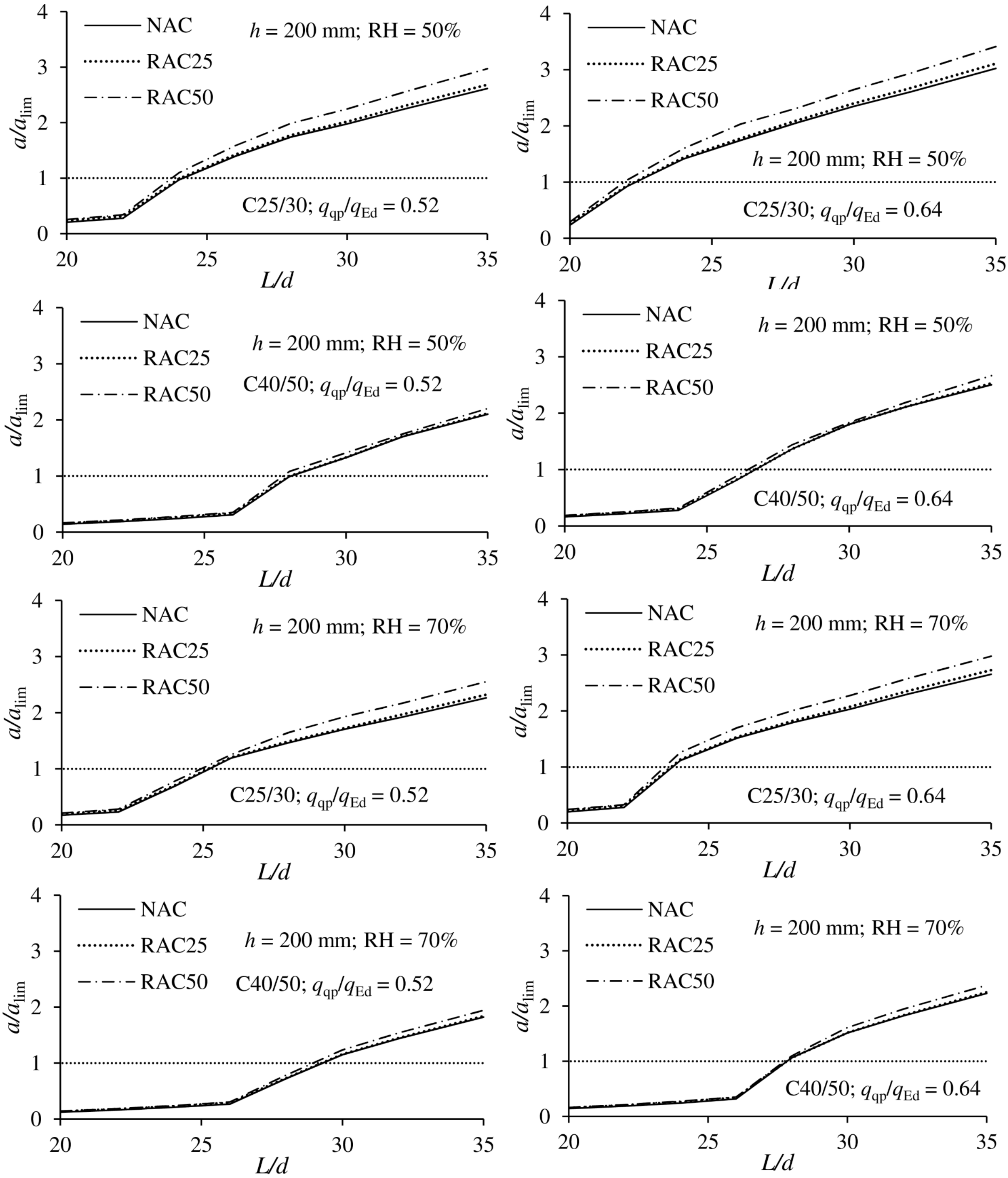

Figure S1. Relationship between $a/a_{\lim}$ and L/d ratios for a simply supported one-way slab with h = 200 mm

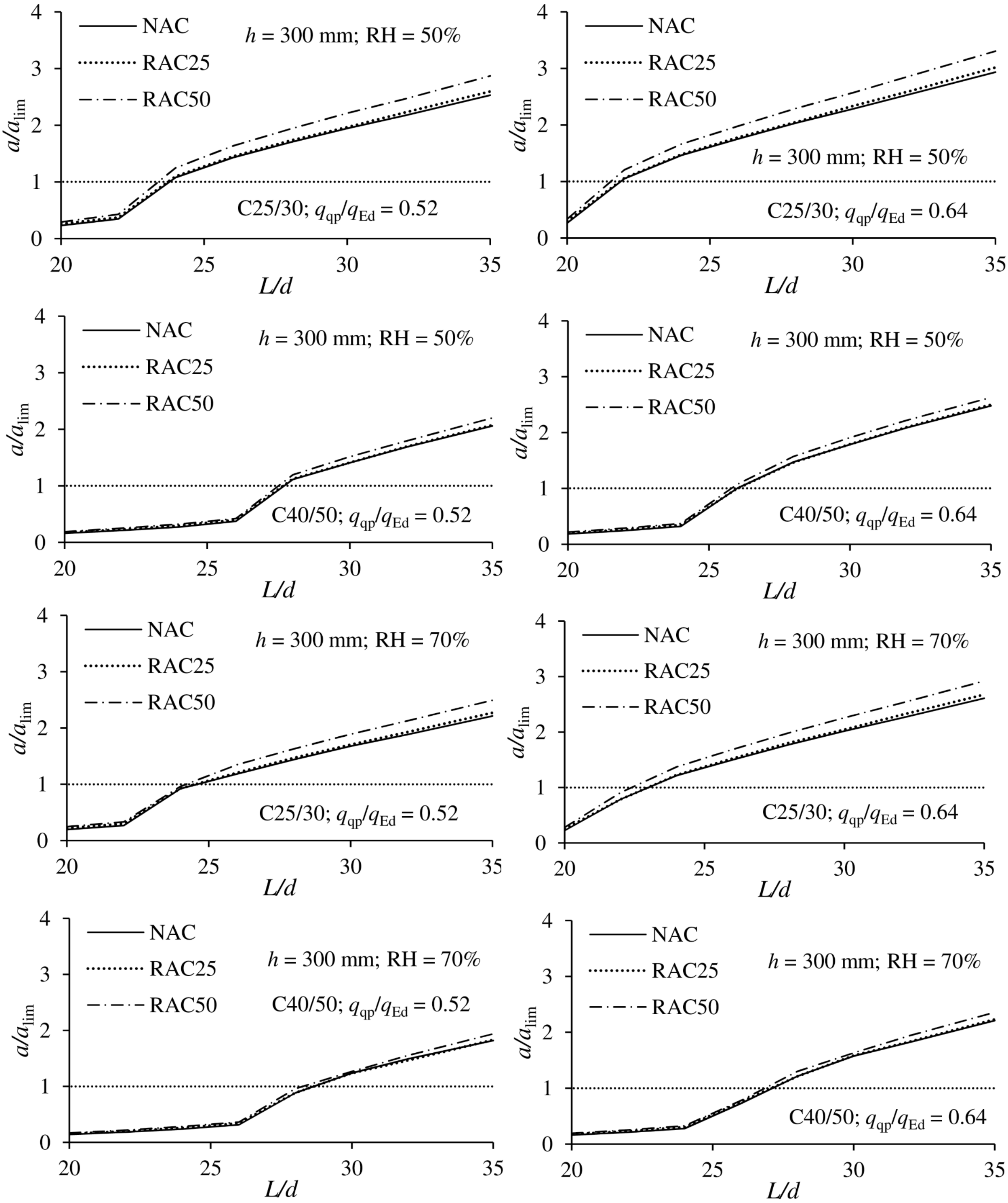

Figure S2. Relationship between a/a_{lim} and L/d ratios for a simply supported one-way slab with h = 300 mm

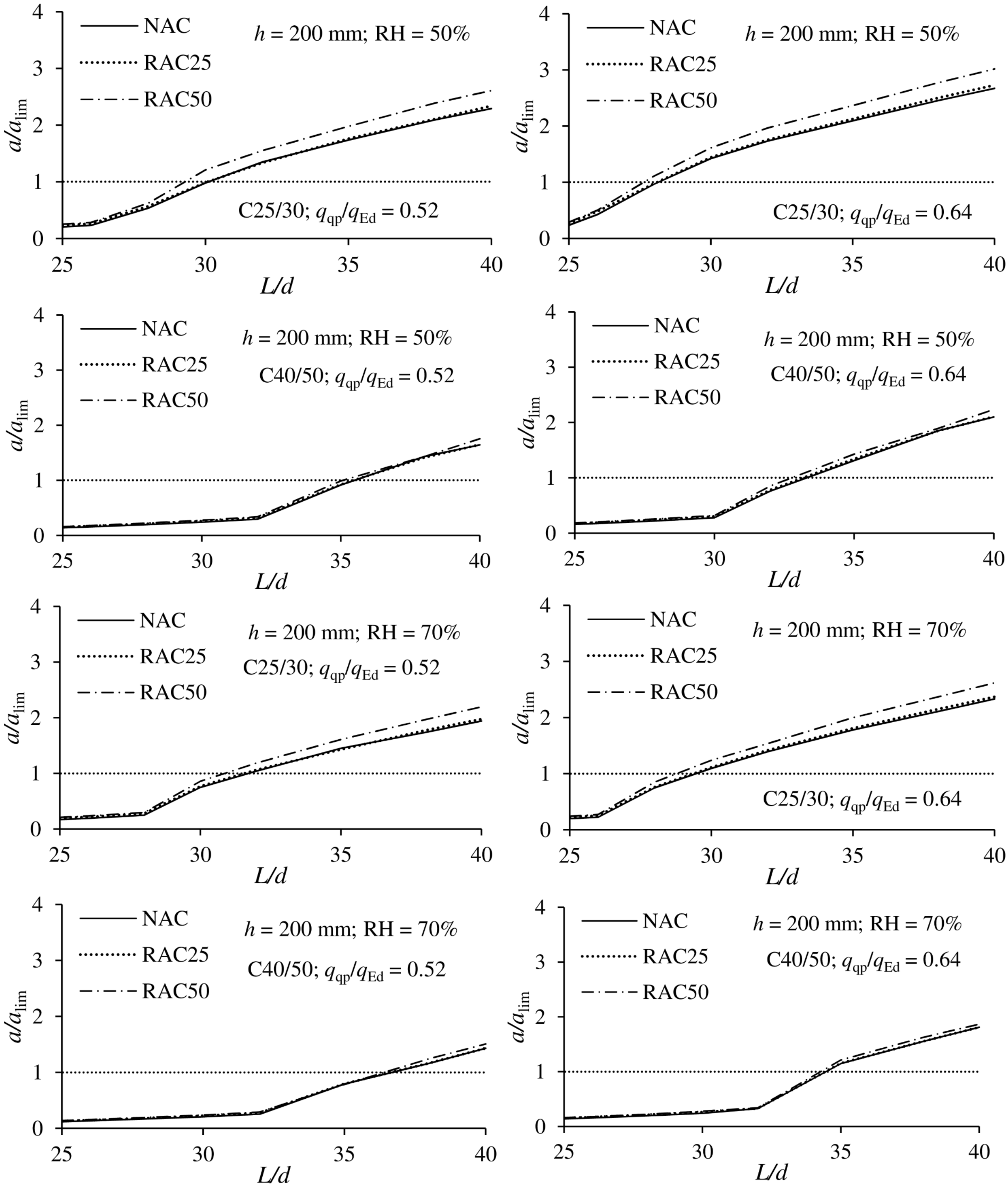

Figure S3. Relationship between a/a_{lim} and L/d ratios for a continuous one-way slab with h = 200 mm

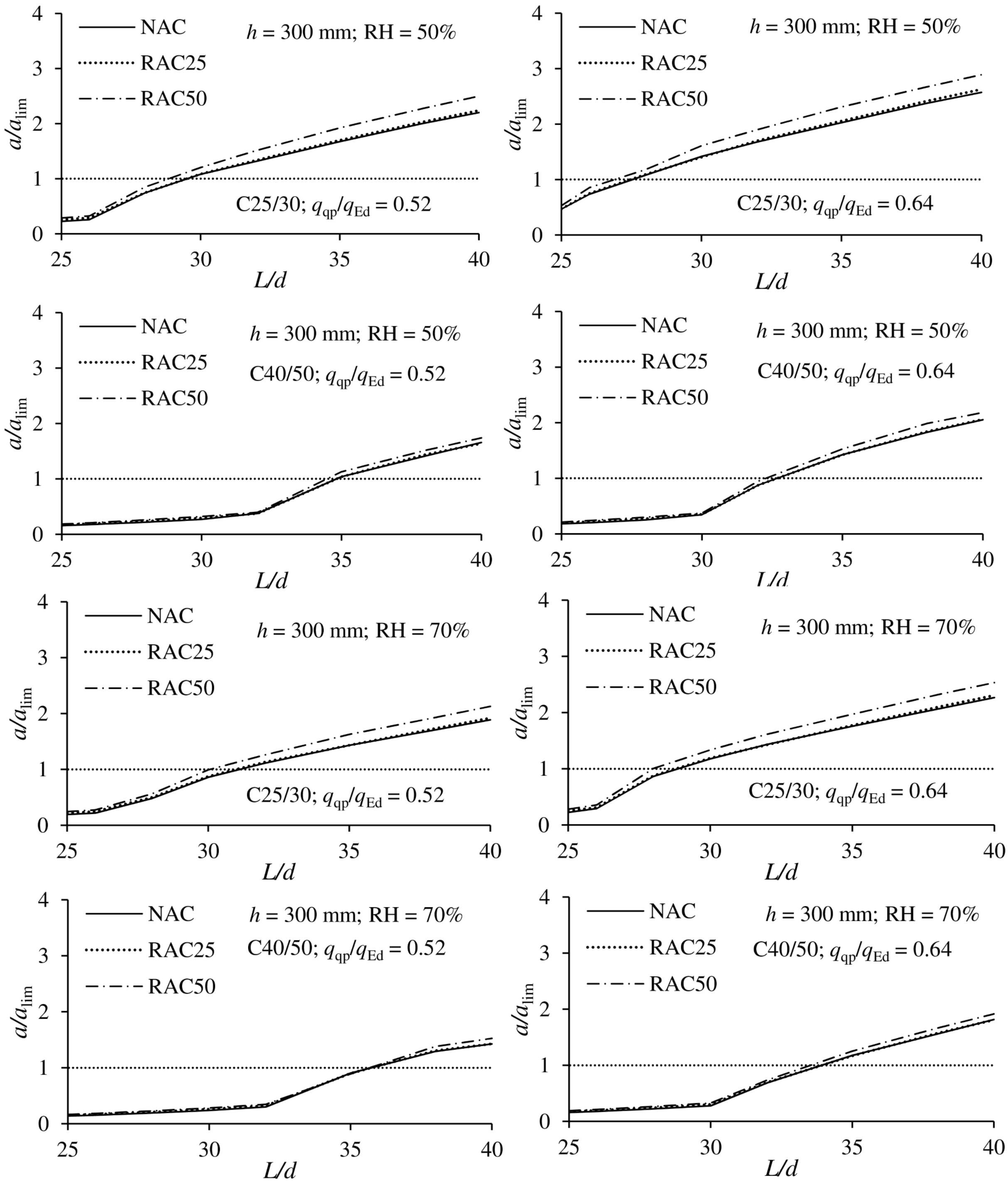

Figure S4. Relationship between a/a_{lim} and L/d ratios for a continuous one-way slab with h = 300 mm

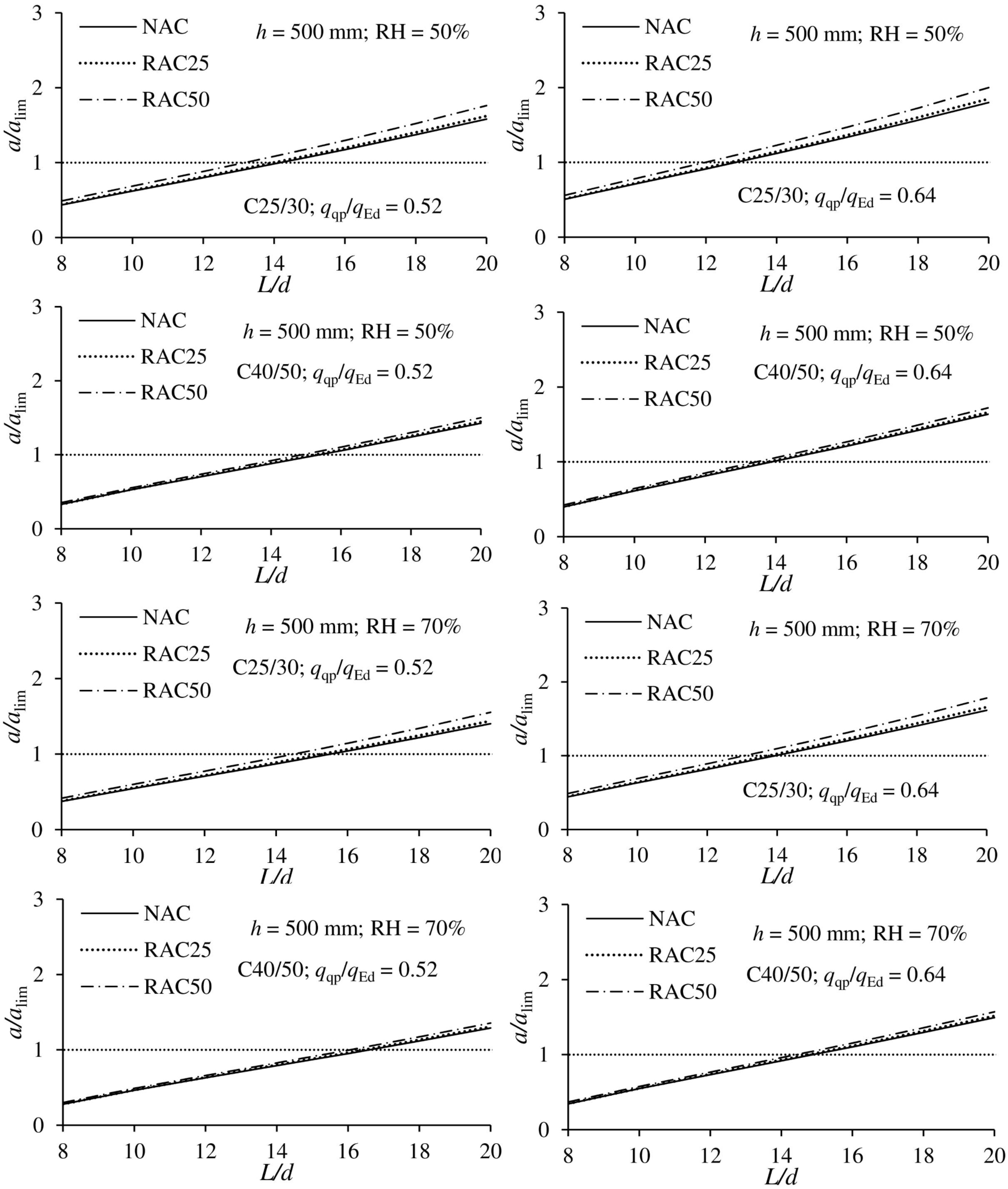

Figure S5. Relationship between a/a_{lim} and L/d ratios for a simply supported T-beam with h = 500 mm

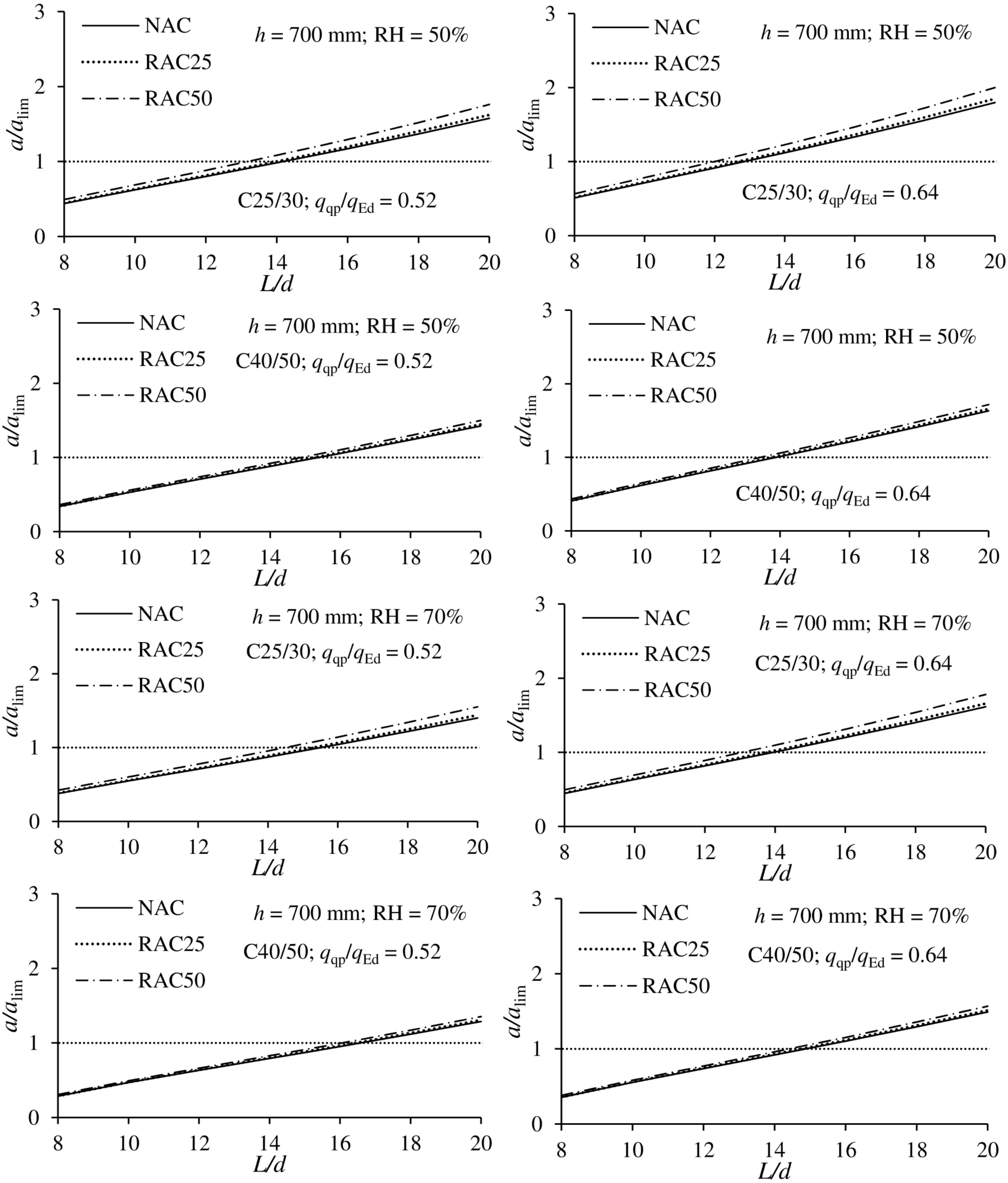

Figure S6. Relationship between a/a_{lim} and L/d ratios for a simply supported T-beam with h = 700 mm

Paper Title: *Parametric numerical study on deflections of reinforced recycled aggregate concrete slabs an*
Journal: *Structural Concrete*
Authors: *Nikola Tošić*[1]
Yahya Kurama[2]
Affiliations: [1] *University of Belgrade, Faculty of Civil Engineering, Bulevar kralja Aleksandra 73, 11000 Be*
[2] *Department of Civil and Environmental Engineering and Earth Sciences, University of Notre*
E-mail: ntosic@imk.grf.bg.ac.rs

ıd beams based on the fib Model Code 2010

ılgrade, Serbia
Dame, Notre Dame, IN, USA

Parameters

	1	2	3	4	5	6	7	8	9	10	11	12	13	14	15	16	17	18
	RAC	**q_{qp}/q_{Ed}**	**f_{ck} (MPa**	**RH (%**	**h (mm)**	**L/d**	**b (mm)**	**d (mm)**	**λ (m)**	**g_{sw} (N/mm^2)**	**Δg (N/mm^2)**	**q (N/mm^2)**	**ψ_2**	**A_s (mm^2)**	**f_{cm} (MPa)**	**L (mm)**	**t (days)**	**a_{lim} (mm)**
1	0	0.52	25	50	200	20	1000	170	1.00	5.0	2.8	3.0	0.0	302.0	33.00	3400	9125.0	13.60

			Parameters																	
	1	2	3	4	5	6	7	8	9	10	11	12	13	14	15	16	15	16	17	18
	RAC	**q_{qp}/q_{Ed}**	**f_{ck} (MPa**	**RH (%**	**h (mm)**	**L/d**	**b (mm)**	**d (mm)**	**λ (m)**	**g_{sw} (N/mm^2)**	**Δg (N/mm^2)**	**q (N/mm^2)**	**ψ_2**	**A_{ss} (mm^2)**	**A_{sl} (mm^2)**	**A_{sr} (mm^2)**	**f_{cm} (MPa)**	**L (mm)**	**t (days)**	**a_{lim} (mm)**
1	0	0.52	25	50	200	25	1000	170	1.00	5.0	2.8	3.0	0.0	381.0	230.0	302.0	33.00	4250	9125.0	17.00

Parameters

	1	2	3	4	5	6	7	8	9	10	11	12	13	14	15	16	17	18	19	20	21
	RAC	q_{qp}/q_{Ed}	f_{ck} (MPa	RH (%	h (mm)	L/d	b (mm)	b_{eff} (mm)	h_f (mm)	d (mm)	λ (m)	g_{sw} (N/mm)	Δg (N/mm)	q (N/mm)	ψ_2	A_{sb} (mm^2)	A_{st} (mm^2)	f_{cm} (MPa)	L (mm)	t (days)	a_{lim} (mm)
1	0	0.52	25	50	500	8	250	2000	150	450	6.00	5.0	2.8	3.0	0.0	757.0	402.0	33.00	3600	9125.0	14.40